

02

The nephelauxetic effect in $\text{ZnAl}_2\text{O}_4:\text{Cr}^{3+}$ nanocrystals induced by their size

© P.J. Dereń, A. Watras, D. Stefańska

Institute of Low Temperature and Structure Research of Polish Academy of Sciences, 50-422 Wrocław, Poland

e-mail: p.deren@intibs.pl

Received July 06, 2021

Revised September 21, 2021

Accepted September 25, 2021

ZnAl_2O_4 nanocrystallites doped with Cr^{3+} ions with mean sizes ranging from 2 to 16 nm were synthesized by the hydrothermal method. Chromium ions occupy the aluminum positions, which symmetry depends on the crystallite size. The smallest nanocrystals have a much larger unit cell than the bigger ones. The metal to ligand distance increases when the size of the nanocrystals decreases. This causes the nephelauxetic effect, which is for the first time (to our knowledge) observed as a size effect. It was also observed that $\text{ZnAl}_2\text{O}_4:\text{Cr}^{3+}$ nanocrystals with size larger than 10 nm possesses the same spectroscopic properties as monocystal.

Keywords: nephelauxetic effect, nanocrystallites, hydrothermal method, ZnAl_2O_4 .

DOI: 10.21883/EOS.2022.01.52997.32-21

Introduction

Size effects in nanoscale materials manifest themselves not only in the spectacular form of „quantum size effects“ but also in melting point changes [1], enlargement of the size of unit cells — this work, or changes in the symmetry of the nanocrystals [2,3]. The main cause of these effects is the influence of surface energy. Many publications have been devoted to research on the surface energy of nanoparticles, previously understood as surface tension [4]. Among them, it should be noted the review article by Vollath et al. [5]. The authors indicate the source of the change in surface energy, which is a large number of unfinished broken bonds; the smaller the particle, the more such bonds per total number of bonds in the nanocrystal. Therefore, as the particle diameter decreases, the surface energy decreases too.

As we will show in this publication, the decrease in surface energy increases the volume of the unit cell. As a result, the distance metal–ligand (here Cr–O) increases and consequently, the strength of the crystal field decreases, the position of the excitation and emission bands shifts, as well as the parameters of Racah change, which ultimately manifests itself as the nephelauxetic effect.

The „nephelauxetic“ in Greek means an expanding cloud. This term was introduced in 1962 by Jørgensen [6] to describe the expansion of the 3d electron cloud when an ion is located in a crystal structure. In a free metal ion, electrons are attracted to the nucleus, but in solids, they participate in bonds with ligands and diffuse out from the nucleus. Therefore, the electrostatic repulsion between these electrons is weaker, and the Racah interelectronic repulsion parameter B decreases. Jørgensen proposed a simple and useful phenomenological description of this effect [6]:

$$B = \beta B_0, \quad (1)$$

where B_0 is the Racah parameter of the free ion and β is the coefficient of proportionality called the nephelauxetic parameter. Brik et al. [7] noticed some limitations of the description proposed by Jørgensen, which reduces the description of the inter-electron interaction to an independent parameter B , assuming that Racah parameter C changes in an identical ratio. This is not true, as the parameters B and C have largely independent values and are subject to varying degrees of reduction due to the interaction with the crystal matrix. Thus, an extended form of the nephelauxetic parameter has been proposed which takes into account both the Racah B and C parameters, namely [7]:

$$\beta_1 = \sqrt{\frac{B}{B_0} + \frac{C}{C_0}}, \quad (2)$$

where C_0 is the Racah parameter of the free ion.

Renata Reisfeld wrote several basic papers and books [8,9] concerning nephelauxetic effect. Her pioneer articles concern either rare earth ions [10] or transition metal ions [11,12]. There are articles both experimental and theoretical ones dedicated to the nephelauxetic effect, some authors apply the external pressure to tune the strength of the mutual electronic repulsion by decreasing metal–ligand distance, others change this distance by adding dopants to the host [13–15].

To study this effect triggered by the weakening of the surface energy, $\text{ZnAl}_2\text{O}_4:\text{Cr}^{3+}$ nanoparticles synthesized by the hydrothermal method were prepared. Spectroscopic properties of the single-crystal $\text{ZnAl}_2\text{O}_4:\text{Cr}^{3+}$ was already published in the 60s of the 20th century [16], a detailed study of so-called N -lines observed in Cr^{3+} emission was published by Mikenda et al. [17–20], recently the spectroscopic properties of $\text{ZnAl}_2\text{O}_4:\text{Cr}^{3+}$ of 80–90 nm have been published [21].

Here, we show the results of our observation of how lowering the size of nanocrystals influences the surface energy and hence the nephelauxetic effect in a compound under normal conditions without applying the high external pressure. To our knowledge, this is the first report, which attributes the nephelauxetic effect to the size of the crystallites and also describes the spectroscopic properties of $\text{ZnAl}_2\text{O}_4:\text{Cr}^{3+}$ nanocrystals whose average diameter is as small as 2.2–16.5 nm.

Experimental

The ZnAl_2O_4 samples doped with Cr^{3+} ions were prepared using microwave-assisted hydrothermal method [22,23]. As precursors powdered hydrated zinc acetate and aluminum isopropoxide were used, dissolved in distilled water with continuous stirring. Then powdered chromium nitride dissolved in distilled water was added. The mixture was stirred for a few minutes and then was poured into a reaction vessel. The microwave hydrothermal reaction were carried out in 200°C , under pressure of 40 bar and for the hold time 30 min. White sol was obtained, later filtered and washed in acetone and then particles of ZnAl_2O_4 were separated by centrifugation. The product thus obtained was dried at a temperature of 120°C and then divided into six portions, five of which were annealed at temperatures of 300, 500, 700, 800, and 900°C , respectively. For all temperatures i.e. from 120 to 900°C , samples doped with 0.1, 0.2, 0.5, and 1% Cr^{3+} were prepared.

Powder diffraction data were collected on an X'Pert PRO X-ray diffractometer with PIXcel ultra-fast line detector, focusing mirror and Soller slits for $\text{CuK}\alpha$ radiation. The diffraction patterns were collected at room temperature in transmission mode in the range of $10^\circ \leq 2\theta \leq 85^\circ$ using step scans of 0.026° . The peak profiles were fitted with the pseudo-Voigt function.

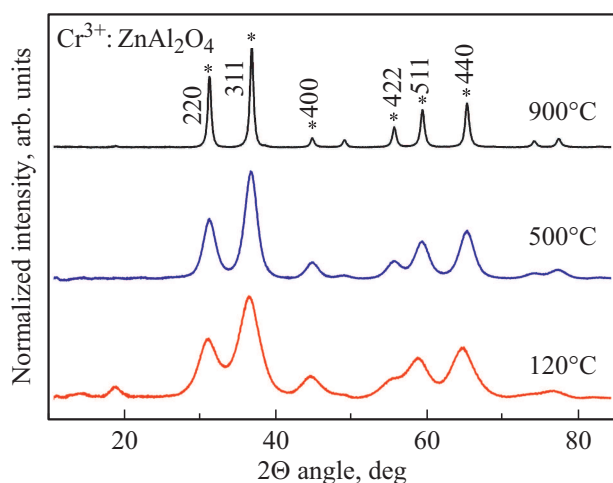


Figure 1. Diffraction patterns of $\text{Cr}^{3+}:\text{ZnAl}_2\text{O}_4$ nanopowder at room temperature; * is position of the Bragg reflections used to calculate the grain size and refine the unit cell.

The emission spectra were measured on Jobin-Yvon HR1000 monochromator. As a detector we used Hamamatsu R928S photomultiplier tube. For excitation an argon and He-Ne lasers were used. The excitation spectra were recorded on SLM AMINCO SPF-500 Spectro-fluorometer. To measure decay profiles we used digital oscilloscope LeCroy WaveSurfer 400 and 532 nm line of pulsed Nd:YAG laser as well as Ti-Sapphire one pumped by the second harmonic Nd:YAG laser as the excitation sources. The samples were cooled in a liquid nitrogen Dewar flask and in a close-cycle He cryostat. To measure calibrated excitation spectra and absolute quantum efficiency we used the C9920 03G system by Hamamatsu.

Further in the text we will apply expression: „the 900°C sample“ for: „the $\text{ZnAl}_2\text{O}_4:\text{Cr}^{3+}$ nanocrystals sample annealed at 900°C “ as well as for any other annealing temperature.

Results

The XRD patterns for selected samples are shown in Fig. 1. All the diffraction lines can be indexed in the cubic spinel structure (space group $\overline{\text{Fd-3m}}$, № 227) without any trace of impurities. The position of the peaks and their shape do not depend on the chromium concentration and are the same in the range of 0.1–1% of dopants. To be consistent with the main topic of this publication, we will only present the data collected for the lowest chromium concentration.

Please note that even the unannealed sample obtained after drying of the sol at 120°C exhibits a ZnAl_2O_4 structure. The most noticeable feature of the diffractograms is the broadening of the Bragg peaks as the annealing temperature decreases. The line profile analysis allowed us to follow the evolution of the mean size of crystallites. We determined the average size of crystallites using the Hall-Williamson approach [24] for six, most separated reflections. As a result, very low values of mean crystallite size were obtained (see Fig. 2). This method is based on the full-width at half maximum (FWHM) of the diffraction peaks and allows additionally to separate the size broadening from the strain-induced broadening of the peaks. In the case of our samples, the peak broadening is dominated by the crystallite size and the micro-strain contribution to the broadening is negligible. Additionally, calculations applying the Hall–Williamson method exhibited very low values of the micro-strain (ca. 0.01% for all the samples). The mean size of the grains grows exponentially with the annealing temperature increase.

The $\text{FW}_{1/5}^{4/5}$ procedure [25] is an extension of the Scherrer method for polydisperse powders and makes it possible to estimate the average size of crystallites as well as the dispersion of a particle size distribution from peak widths measured at 1/5 and 4/5 of the maximum. We used the line (400) because it was well separated for samples with a sintering temperature $\geq 300^\circ\text{C}$. This method gives

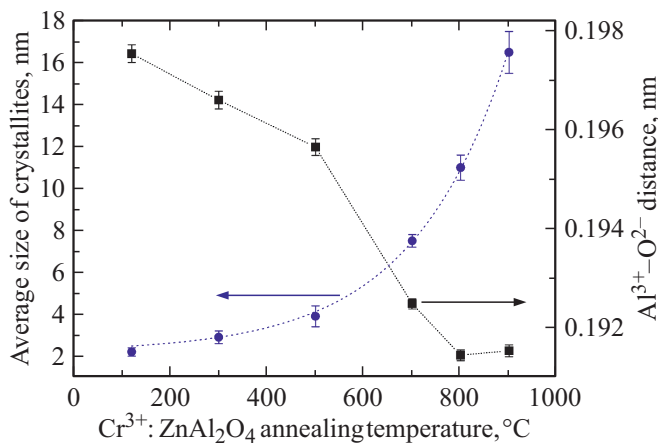


Figure 2. Average crystallite size and $\text{Al}^{3+}-\text{O}^{2-}$ distance vs. annealing temperature (see details in text).

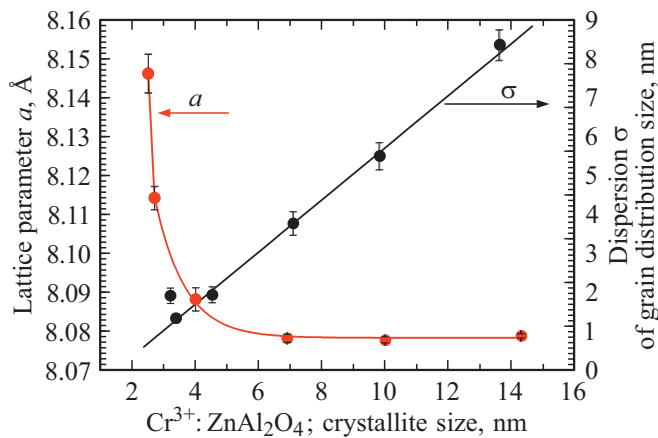


Figure 3. Lattice parameter a (red circles) and dispersion σ of grain distribution size (black circles) vs. crystallite size.

similar values of the grain size, the values are shown in Fig. 3. The dispersion σ of the average crystallite size shows linear growth with an increase in the average grain size. For low sintering temperatures (mean crystallite size < 4 nm), the crystallite size distribution is narrow while at higher sintering temperatures it is at least 2 times larger.

TEM measurements confirmed the calculated values of grain size. It can be seen that the grains of the 120°C sample are smaller than 5 nm (Fig. 4, *a*) and have a spherical shape, while the grains of the 900°C sample have a diameter of about 15–20 nm and their shape is more elongated (Fig. 4, *b*). In the inset of Fig. 4, *a*, the Selected Area Electron Diffraction (SAED) is shown. The electron beam was directed into small black spots seen in Fig. 4, *a* representing ZnAl_2O_4 nanoparticles. The observed diffraction rings confirm the crystallographic cubic structure of these particles. The unit cell parameter was calculated from the least-squares refinement of six best-separated peaks. The results are shown in Fig. 3. The lattice

parameter increases with decreasing particle size especially when the particle size is less than 6 nm.

Emission spectra were recorded at the room, liquid nitrogen temperature and at 10 K. For all annealing temperatures emission from the 2E_g level — so-called R-lines and N-lines are present, but emission lines of the samples annealed below 700°C are broad (see Fig. 5).

Those annealed at 900°C have almost identical emission as presented by Wood and Imbush [16] and Mikenda et al. [17–19] for a single crystal. Since other authors assigned them carefully we will not repeat their work here. The reader may find in mentioned above papers a comprehensive analysis of the N-line origin. Detailed analysis of the emission shows however that the position of all lines exhibits a blue shift with decreasing the crystalline size, for example the R1 line shifts from 14573 to 14583 cm^{-1} (see Fig. 6). The R splitting, measured at 10 K, increases with decreasing of the crystallite size and for the 900°C sample $\Delta R = 6.0\text{ cm}^{-1}$, while for the 700°C is 9.8 cm^{-1} , and finally, for the 120°C sample $\Delta R = 19.2\text{ cm}^{-1}$. The N_1 - and N_2 -lines increase their intensity for small nanocrystals.

Emission decay profiles of the 900°C sample measured at 77 K are single exponential and the decay times obtained follow those presented by Wood [16] or Mikenda [17–19] (see Fig. 7, *a*) although the emission decay times are much longer than reported by them. For example, the R-line of the 900°C sample doped with 0.1% Cr^{3+} at room temperature decays with 33 ms constant, while for 77 K and 10 K registered decay time was 43 and 50 ms, respectively (see Fig. 7, *b*), though Wood reports only 29 and 31 ms, respectively for the same Cr^{3+} concentration [16]. Please note that the emission decay time is size-dependent, for the smallest nanocrystallites it equals only 10 ms at 300 K (see Fig. 7, *b*).

The excitation spectra monitored on the R-lines show a very interesting characteristic, their shape, and their position depend on the size of the nanocrystallites (see Fig. 8). There is a redshift of the 4T_2 and 4T_1 band observed as the size of the nanocrystallites decreases. The crystal field parameters Dq and the interelectronic repulsion parameters of Racah B and C were calculated taking data from the excitation and emission spectra by solving the equation set:

$$\begin{aligned} \nu_1 &= 10Dq, \\ \nu_2 &= \frac{1}{2}(15B + 30Dq) \\ &\quad - \frac{1}{2}[(15B - 10Dq)^2 + 12B \cdot 10Dq]^{1/2}, \\ \nu_3 &= 3.05C - 1.8B^2/Dq + 7.9B, \end{aligned} \quad (3)$$

where ν_1 , ν_2 and ν_3 are energies of the ${}^4T_{2g}$, ${}^4T_{1g}$ and 2E_g levels, respectively. Dq/B as well as the Racah parameter B are shown in Fig. 9. Dq/B parameter is decreasing when the nanocrystal size decreases, while B parameter increases. The ${}^4T_2/{}^4T_1$ integrated intensity ratio changes also because the intensity of the 4T_1 band decreases when annealing temperature increases (see Fig. 10).

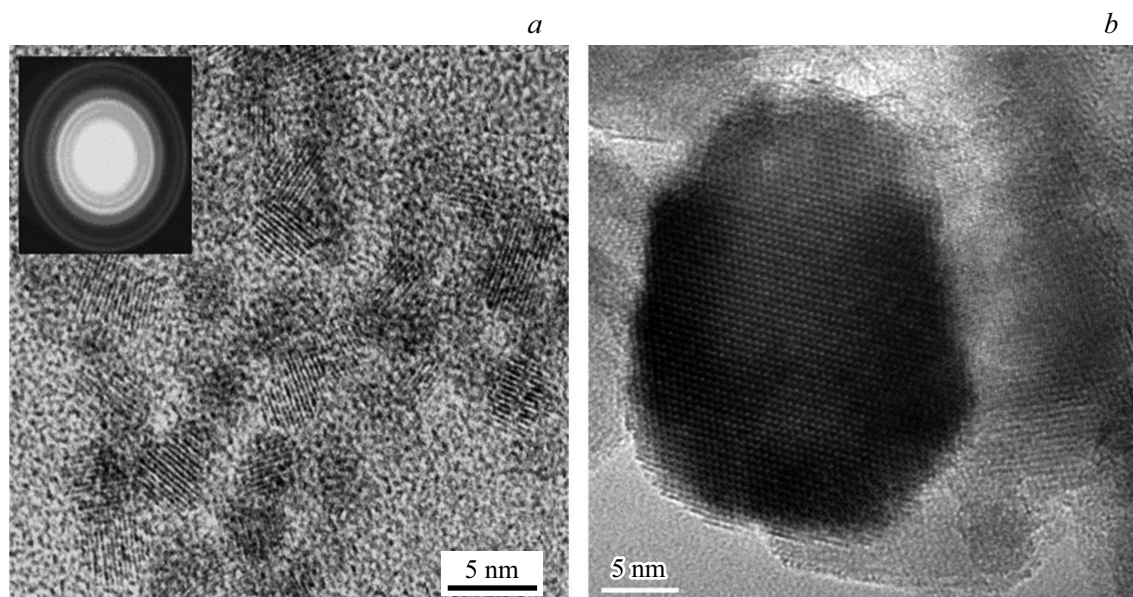


Figure 4. TEM images of samples 120°C (a) and 900°C (b). The insert shows SAED spectrum of sample 120°C.

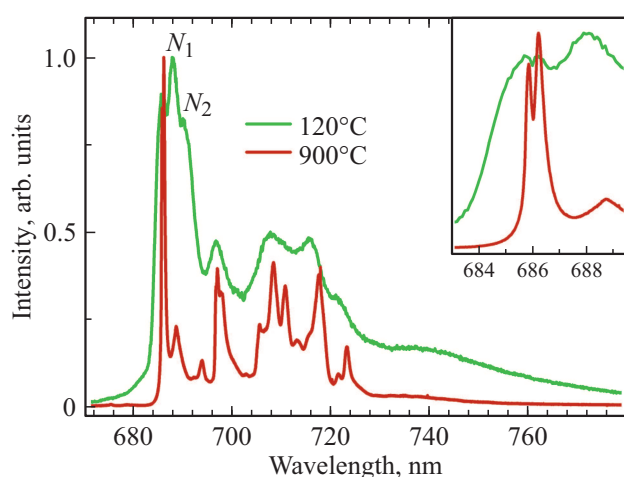


Figure 5. Luminescence spectra of ZnAl₂O spinel doped with 0.1% Cr³⁺ at 10 K, $\lambda_{\text{exc}} = 514.5$ nm.

Discussion

When a Cr³⁺ ion is in the $^4A_{2g}$ ground state, three 3d electrons occupy the d_{xy} , d_{xz} and d_{yz} orbitals. These orbitals are pointed between the ligands, so this level is less sensitive to the crystal field than those of 4T_2 and 4T_1 . The first and second states of the excited quartet have the same $t_{2g}^2 e_g^1$ electronic configuration, but they differ in their orbitals. The lower $^4T_{2g}$ applies the d_{xz} , d_{yz} , and $d_{x^2-y^2}$ orbitals. The second quartet $^4T_{1g}$ consists of the d_{xz} , d_{yz} and d_{z^2} orbitals. The $d_{x^2-y^2}$ and d_{z^2} orbitals point to the ligands, so both levels are very sensitive to the metal-ligand distance (M–L).

Once the ligands approach the metal ion, which could be forced by the external pressure, the bonds become more covalent, the 3d electrons spread further and the parameter

B decreases, the energies of the states of the quartet change drastically. Because the 2E_g level has the same electronic configuration as the ground state, its energy is much less sensitive to changes in the crystal field, so the nephelauxetic effect is much less pronounced than for quartet states. However, the position of the line R changes as well as the energy gap ΔR between the components R_1 and R_2 (see Fig 6).

The energy separation between $^4A_{2g}$ and $^4T_{2g}$ equal to $10Dq$ is considered as the strength of the octahedral crystal field. The Racah B and C mutual repulsion parameters are calculated taking into account the energy of the quartets $^4T_{2g}$, $^4T_{1g}$ and the doublet 2E_g . The increasing value Dq/B (see Fig. 9, b) with increasing crystallite size indicates the increasing strengths of the crystal field. By definition, the nephelauxetic effect is manifested by a reduction in the

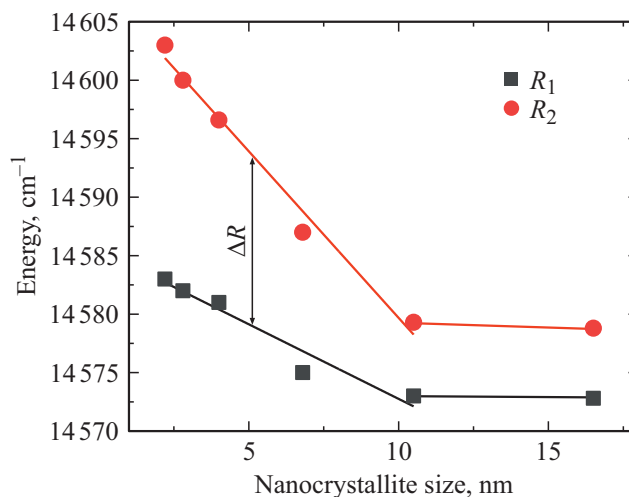


Figure 6. Position of R -lines vs. nanocrystallite size.

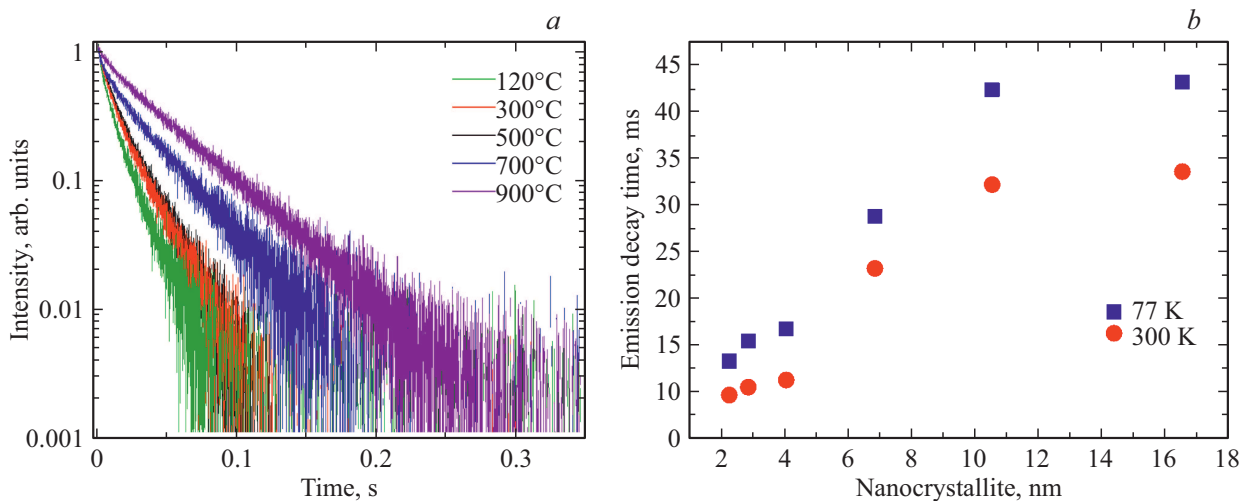


Figure 7. (a) is amplitude decay of the R-line of samples $\text{ZnAl}_2\text{O}_4:\text{Cr}^{3+}$ (0.1%) vs. annealing temperature, $\lambda_{\text{exc}} = 532$ nm, $T = 77$ K, (b) is radiation decay times for samples $\text{ZnAl}_2\text{O}_4:\text{Cr}^{3+}$ (0.1%) vs. nanocrystallite size.

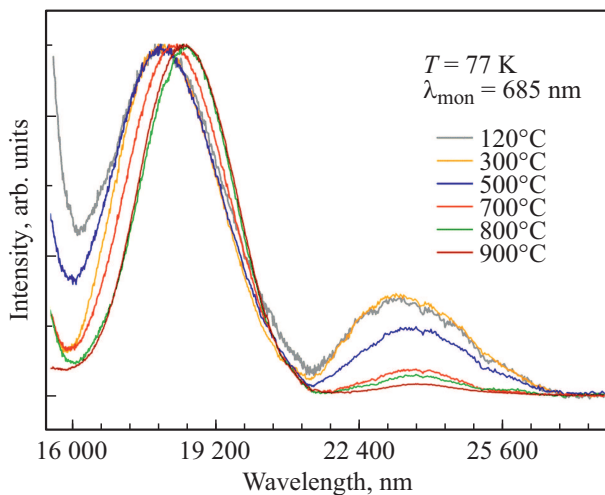


Figure 8. Excitation spectra recorded on the R-line at 77 K for samples $\text{ZnAl}_2\text{O}_4:\text{Cr}^{3+}$.

Racah parameter B and an increase in C when the distance $M-L$ decreases (see Fig. 9, a), that is to say with the increase in the size of the crystallites. The β_1 as a function of the size of the crystallites is plotted in Fig. 11. It changes in the same way as the classical parameter β but in a more linear manner. Please note that changes are observed only in the 2–10 nm range; nanocrystallites possessing 10 nm size exhibit the same value of the nephelauxetic parameter as the ZnAl_2O_4 single crystal.

The very long decay time in nanocrystal comparing to bulk crystal was explained in terms of the effective index of refraction n_{eff} [26] defined as follows:

$$n_{\text{eff}}(x) = xn_{\text{sample}} + (1-x)n_{\text{med}}, \quad (4)$$

where x is the „filling factor“ and n_{med} is the refractive index of the surrounding nanoparticle medium. Since

radiative decay time is proportional to refractive index i.e. $\tau_R \approx 1/n(n^2 + 2)^2$ any change of the n will affect dramatically the decay time which is much longer when a sample grain diameter is of the order of nanometers. For the 900°C samples, emission decay time was 43 ms. Since Wood et al. [16] reported 31(± 2) ms as decay time of ZnAl_2O_4 single crystal, calculated parameter $x = 0.69$ for such small nanoparticles seems to be a reasonable value.

Emission decay time depends on nanocrystallite size and decreases with size decreasing (see Fig. 7, b). This could be associated with either a smaller degree of crystallinity or lower site symmetry of the Cr^{3+} ions. The small (2–3 nm) nanocrystals are formed by only a dozen gahnite unit cells, the largest studied consist of at least 10^4 unit cells. For the former nanocrystallites, most of the unit cells are on the nanocrystallites surface, contrary to the „bigger“ ones. Nanocrystallites annealed at higher temperature and thus possessing bigger size have also smaller unit cells and much „better organized“ surrounding than smaller ones in the sense that their structure is much closer to ideal cubic symmetry than in the smallest nanocrystals. Very long (43 ms) decay time indicates high site symmetry and magnetic dipole origin of the emission.

Increased symmetry is manifested also by smaller R-line splitting for the bigger nanocrystals (see Fig. 6). When chromium is situated in the ideal cubic site in the center of inversion the R line exhibit no splitting [18]. When a local symmetry decreases the splitting ΔR of the R-line increases. The smallest $\Delta R = 6.75$ cm^{-1} was observed for the 900°C samples, then with decreasing annealing temperature increases to 20 cm^{-1} .

In general, when the distortion from the octahedral symmetry increases the splitting increases too (see Fig. 6), for comparison in Ruby ΔR is equal to 29 cm^{-1} , 47 cm^{-1} in YAlO_3 , and in emerald 63 cm^{-1} , one of the larger

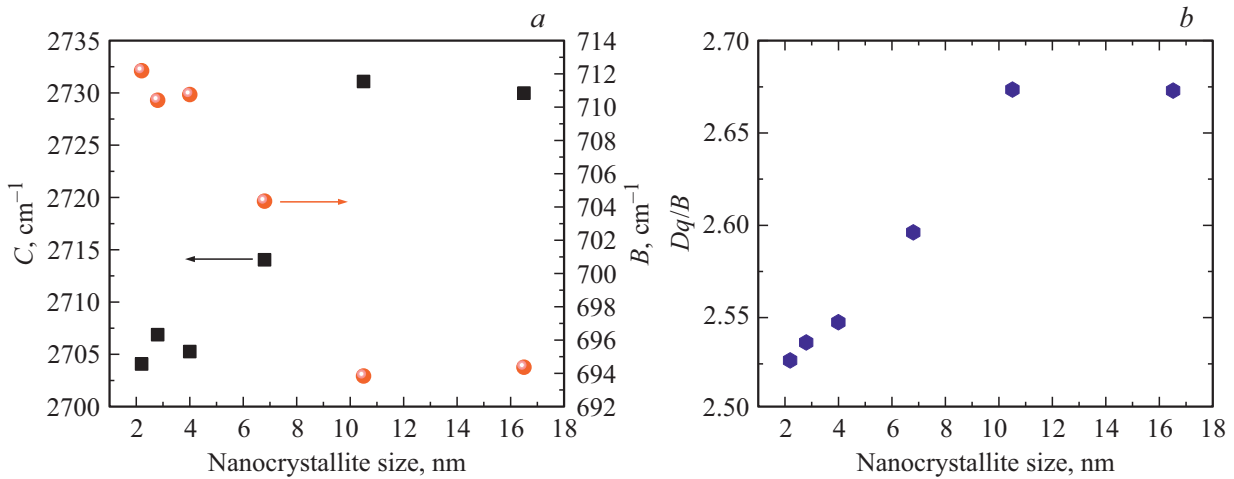


Figure 9. (a) is Racah parameters B and C (red circles and black squares, respectively), (b) is parameter Dq/B depending on the nanocrystallite size $\text{ZnAl}_2\text{O}_4:\text{Cr}^{3+}$.

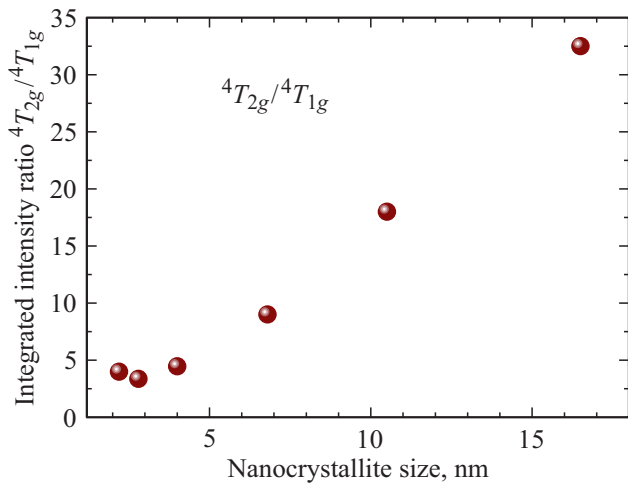


Figure 10. Integral ratio of intensities ${}^4T_2/{}^4T_1$ depending on the size of ZnAl_2O_4 nanocrystals.

splitting was noticed for Ga_2O_3 — 156 cm^{-1} . Since ΔR is proportional to the distortion from the ideal cubic symmetry it could be regarded as a measure of this distortion.

Dependence of the ${}^4T_2/{}^4T_1$ integrated intensity ratio on $\text{Cr}^{3+}-\text{O}^{2-}$ distance (see Fig. 10) is a very strong indication of the chromium site symmetry changes. This ratio increases when the nanocrystallite diameter increases. Changes in the intensity ratio of the quartet bands were observed already for MgO [27] and MgAl_2O_4 [28]. The same behavior was observed for $\text{Cs}_2\text{NaGaF}_6$ [29], but no one has pointed that it is due to changes in local Cr^{3+} symmetry. Two groups of sites are present in MgO crystal one has low whereas the second has high symmetry cubic site. For the later ${}^4T_2/{}^4T_1$ ratio is 3.7 for the former 1.15 (see excitation spectra in [27]). For the elpasolite mentioned above this ratio is about 2. The same tendency is observed for the ZnAl_2O_4 nanocrystallites. For larger nanocrystals, the Cr^{3+}

ions are located at a higher symmetry site than in smaller ones. At a higher symmetry site, the probability of the ${}^4A_2 \rightarrow {}^4T_2$ transition increases over the probability of the ${}^4A_2 \rightarrow {}^4T_1$ transition.

Conclusions

ZnAl_2O_4 nanocrystals were synthesized by the hydrothermal method. Their structure was confirmed by the XRD spectra and TEM measurements. Nanocrystals obtained at 120°C have an average diameter of 2.2 nm, which increases with the annealing temperature and is about 16 nm for the 900°C sample. The smallest nanocrystallites have the largest unit cell as well as the doped Cr^{3+} has the largest distance to the ligands. The unit cell and $\text{Cr}-\text{O}$ distance decrease with increased annealing temperature and for the 900°C sample is the same as in ZnAl_2O_4 bulk. Smaller distances increase the strength of the crystal field, the Dq/B

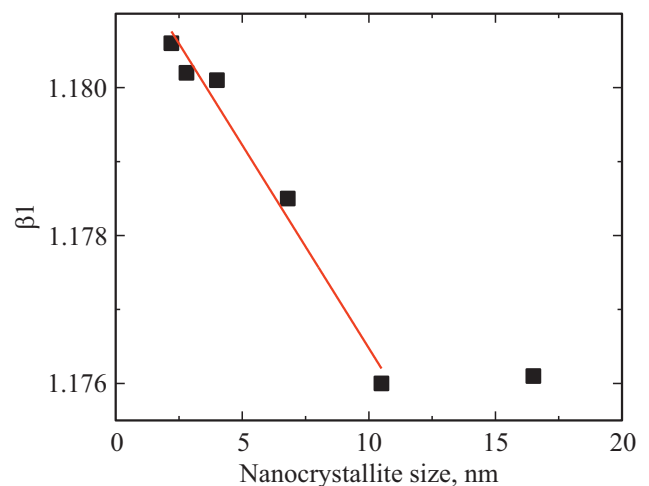


Figure 11. Nephelauxetic parameter β_1 calculated by formula (2) as a function of crystallite size.

changes from 2.52 for the smallest nanocrystals to 2.67 for the largest ones.

In bigger nanocrystallites, Cr^{3+} ions are located at higher symmetry sites, in smaller nanocrystals where the unit cell is bigger than in the bulk the Cr^{3+} ions are located at distorted cubic symmetry sites. This is manifested by larger ΔR splitting, lower ${}^4T_2/{}^4T_1$ intensity ratio, and shorter decay time. The nephelauxetic effect in $ZnAl_2O_4$ nanocrystals is manifested by change of the Racah B parameter, which decreases with the increase of Cr–O distance.

It is possible to summarize the results presented in this paper by the conclusion that nano-crystallites with sizes greater than 10 nm have already the same spectroscopic properties as those presented for the large single crystal. The reduction in their size leads to much greater interaction of surface energy forces as there are fewer and fewer unit cells inside the crystallite nucleus and proportionally the number of unit cells on the surface of the crystallite increases. This results in an increase in the unit cell volume and in the distances between ligands and dopants ions, and consequently in a weakening of the ligand field. Eventually, this manifests itself as the nephelauxetic effect. The evolution of the Racah parameters and the parameter β , decay times is linear as a function of the size of the crystallites.

Acknowledgments

The authors thank Dr. hab. Anna Gągor for XRD measurements and Dr. Michalina Kurnatowska for TEM measurements.

Conflict of interest

The authors declare that they have no conflict of interest.

References

- [1] P.D. Cluskey, R.J. Newport, R.E. Benfield, S.J. Gurman, G. Schmid. *Zeitschrift Fur Phys. D Atoms, Mol. Clust.*, **26**, 8 (1993). DOI: 10.1007/BF01425601
- [2] P.J. Dereń, K. Lemański, A. Gągor, A. Watras, M. Małecka, M. Zawadzki. *J. Solid State Chem.*, **183**, 2095 (2010). DOI: 10.1016/j.jssc.2010.07.015
- [3] P.J. Dereń, K. Lemański. *J. Lumin.*, **131**, 445 (2011). DOI: 10.1016/j.jlumin.2010.11.035
- [4] J.W. Gibbs. *The scientific papers of J. Willard Gibbs*, Vol. 1 (Yale University Press, New Haven, 1957).
- [5] D. Vollath, F.D. Fischer, D. Holec, F. D. Beilstein. *J. Nanotechnol.*, **9**, 2265 (2018). DOI: 10.3762/bjnano.9.211
- [6] C.K. Jørgensen. *Prog. Inorg. Chem.*, ed. by F.A. Cotton (Interscience Publishers, New York, London, 1962), p. 73–124.
- [7] M.G. Brik, S.J. Camardello, A.M. Srivastava, N.M. Avram, A. Suchocki. *ECS J. Solid State Sci. Technol.*, **5**, R3067 (2016). DOI: 10.1149/2.0091601jss
- [8] R. Reisfeld, C.K. Jørgensen. *Lasers and Excited States of Rare Earths* (Springer, Berlin, Heidelberg, 1977). DOI: 10.1007/978-3-642-66696-4
- [9] R. Reisfeld, C.K. Jørgensen. *Handbook on The Physics and Chemistry of Rare Earths*, (Elsevier, 1987) Ch. 58, p. 1–90. DOI: 10.1016/S0168-1273(87)09004-4
- [10] R. Reisfeld, J. Hormodaly, B. Barnett. *Chem. Phys. Lett.*, **17**, 248 (1972). DOI: 10.1016/0009-2614(72)87066-0
- [11] R. Reisfeld, L. Boehm. *J. Non. Cryst. Solids*, **17**, 209 (1975). DOI: 10.1016/0022-3093(75)90051-4
- [12] R. Reisfeld, L. Boehm. *J. Non. Cryst. Solids*, **16**, 83 (1974). DOI: 10.1016/0022-3093(74)90070-2
- [13] P.J. Dereń, A. Watras, A. Gągor, R. Pazik. *Cryst. Growth Des.*, **12**, 4752 (2012). DOI: 10.1021/cg300435t
- [14] A. Suchocki, S.W. Biernacki, M. Grinberg. *J. Lumin.*, **125**, 266 (2007). DOI: 10.1016/j.jlumin.2006.08.039
- [15] A.L. Tchougr'eff, R. Dronskowski. *Int. J. Quantum Chem.*, **109**, 2606 (2009). DOI: 10.1002/qua.21989
- [16] D.L. Wood, G.F. Imbusch, R.M. Macfarlane, P. Kisliuk, D.M. Larkin. *J. Chem. Phys.*, **48**, 5255 (1968). DOI: 10.1063/1.1668202
- [17] W. Mikenda, A. Preisinger. *J. Lumin.*, **26**, 53 (1981). DOI: 10.1016/0022-2313(81)90169-1
- [18] W. Mikenda, A. Preisinger. *J. Lumin.*, **26**, 67 (1981). DOI: 10.1016/0022-2313(81)90170-8
- [19] W. Mikenda. *J. Lumin.*, **26**, 85 (1981). DOI: 10.1016/0022-2313(81)90171-X
- [20] J. Derkosch, W. Mikenda. *J. Lumin.*, **28**, 431 (1983). DOI: 10.1016/0022-2313(83)90010-8
- [21] H.H. Luc, T.K. Nguyen, V.M. Nguyen, A. Suchocki, A. Kaminska, V.K. Le, V.H. Nguyen, T.T. Luong. *Acta Phys. Pol. A*, **104**, 581 (2003). DOI: 10.12693/APhysPolA.104.581
- [22] M. Zawadzki. *Solid State Sci.*, **8**, 14 (2006). DOI: 10.1016/j.solidstatesciences.2005.08.006
- [23] M. Zawadzki. *J. Alloys Compd.*, **439**, 312 (2007). DOI: 10.1016/j.jallcom.2006.08.077
- [24] G. Williamson, W. Hall. *Acta Metall.*, **1**, 22 (1953). DOI: 10.1016/0001-6160(53)90006-6
- [25] R. Pielaszek. *J. Alloys Compd.*, **382**, 128 (2004). DOI: 10.1016/j.jallcom.2004.05.040
- [26] R.S. Meltzer, S.P. Feofilov, B. Tissue, H.B. Yuan. *Phys. Rev. B*, **60**, 12 (1999). DOI: 10.1103/physrevb.60.r14012
- [27] F. Castelli, L. Forster. *Phys. Rev. B*, **11**, 920 (1975). DOI: 10.1103/PhysRevB.11.920
- [28] P. Głuchowski, R. Pazik, D. Hreniak, W. Streck. *Chem. Phys.*, **358**, 52 (2009). DOI: 10.1016/j.chemphys.2008.12.018
- [29] R.J. da Fonseca, A. Tavares, P. Silva, T. Abritta, N. Khaidukov. *Solid State Commun.*, **110**, 519 (1999). DOI: 10.1016/S0038-1098(99)00008-3